Title

18F-flortaucipir tau positron emission tomography distinguishes established progressive supranuclear palsy from controls and Parkinson disease: A multicenter study

Journal

Annals of Neurology, 82(4)

ISSN

0364-5134

Authors

Schonhaut, Daniel R
McMillan, Corey T
Spina, Salvatore
et al.

Publication Date

2017-10-01

DOI

10.1002/ana.25060

Peer reviewed

^{18}F-Flortaucipir Tau Positron Emission Tomography Distinguishes Established Progressive Supranuclear Palsy from Controls and Parkinson Disease: A Multicenter Study

Daniel R. Schonhaut, BA,[1,2,3] Corey T. McMillan, PhD,[3] Salvatore Spina, MD, PhD,[1] Bradford C. Dickerson, MD,[4] Andrew Siderowf, MD,[5] Michael D. Devous Sr, PhD,[5] Richard Tsai, MD,[1] Joseph Winer, BA,[2] David S. Russell, MD, PhD,[6] Irene Litvan, MD,[7] Erik D. Roberson, MD, PhD,[8] William W. Seeley, MD,[1,9] Lea T. Grinberg, MD, PhD,[1,9] Joel H. Kramer, PsyD,[1] Bruce L. Miller, MD,[1] Peter Pressman, MD,[1] Ilya Nasrallah, MD, PhD,[3] Suzanne L. Baker, PhD,[2] Stephen N. Gomperts, MD, PhD,[4] Keith A. Johnson, MD,[4] Murray Grossman, MD,[3] William J. Jagust, MD,[2] Adam L. Boxer, MD, PhD,[1] and Gil D. Rabinovici, MD[1,2]

Objective: ^{18}F-flortaucipir (formerly ^{18}F-AV1451 or ^{18}F-T807) binds to neurofibrillary tangles in Alzheimer disease, but tissue studies assessing binding to tau aggregates in progressive supranuclear palsy (PSP) have yielded mixed results. We compared in vivo ^{18}F-flortaucipir uptake in patients meeting clinical research criteria for PSP (n = 33) to normal controls (n = 46) and patients meeting criteria for Parkinson disease (PD; n = 26).
Methods: Participants underwent magnetic resonance imaging and positron emission tomography for amyloid-β (^{11}C-PiB or ^{18}F-florbetapir) and tau (^{18}F-flortaucipir). ^{18}F-flortaucipir standardized uptake value ratios were calculated (t = 80–100 minutes, cerebellum gray matter reference). Voxelwise and region-of-interest group comparisons were performed in template space, with receiver operating characteristic curve analyses to assess single-subject discrimination. Qualitative comparisons with postmortem tau are reported in 1 patient who died 9 months after ^{18}F-flortaucipir.
Results: Clinical PSP patients showed bilaterally elevated ^{18}F-flortaucipir uptake in globus pallidus, putamen, subthalamic nucleus, midbrain, and dentate nucleus relative to controls and PD patients (voxelwise $p < 0.05$ family wise error corrected). Globus pallidus binding best distinguished PSP patients from controls and PD (area under the curve [AUC] = 0.872 vs controls, AUC = 0.893 vs PD). PSP clinical severity did not correlate with ^{18}F-flortaucipir in any region. A patient with clinical PSP and pathological diagnosis of corticobasal degeneration had severe tau pathology in PSP-related brain structures with good correspondence between in vivo ^{18}F-flortaucipir and postmortem tau neuropathology.
Interpretation: ^{18}F-flortaucipir uptake was elevated in PSP versus controls and PD patients in a pattern consistent with the expected distribution of tau pathology.

ANN NEUROL 2017;82:622–634

View this article online at wileyonlinelibrary.com. DOI: 10.1002/ana.25060

Received Apr 7, 2017, and in revised form Sep 10, 2017. Accepted for publication Sep 24, 2017.

Address correspondence to Dr Rabinovici, University of California, San Francisco, Memory and Aging Center, 675 Nelson Rising Lane, Suite 190, San Francisco, CA 94158. E-mail: gil.rabinovici@ucsf.edu

From the [1]Memory and Aging Center, University of California, San Francisco, San Francisco, CA; [2]Helen Wills Neuroscience Institute, University of California, Berkeley, Berkeley, CA; [3]Perelman School of Medicine, University of Pennsylvania, Philadelphia, PA; [4]Department of Neurology, Massachusetts General Hospital and Harvard Medical School, Charlestown, MA; [5]Avid Radiopharmaceuticals, Philadelphia, PA; [6]Institute for Neurodegenerative Disorders, New Haven, CT; [7]Department of Neurology, University of California, San Diego, San Diego, CA; [8]Department of Neurology, University of Alabama at Birmingham, Birmingham, AL; and [9]Department of Pathology, University of California, San Francisco, San Francisco, CA

Progressive supranuclear palsy (PSP) is a sporadic, atypical parkinsonian disorder with progressive motor and cognitive dysfunction beginning at age 40 years or later. The most common clinical presentation is Richardson syndrome (PSP-RS), noted for early postural and gait instability with falls, vertical gaze palsy, and frontal dementia. This syndrome is associated with underlying neurodegeneration of the basal ganglia, midbrain, pons, and dentate nucleus of the cerebellum, with later involvement of cortex (especially frontal), subcortical white matter (WM), and cerebellar WM.[1,2] In addition, several clinical variants of PSP have recently been identified, including L-dopa–resistant parkinsonism (PSP-P), pure akinesia with gait freezing (PSP-PAGF), corticobasal syndrome (PSP-CBS), nonfluent variant primary progressive aphasia, and behavioral-variant frontotemporal dementia.[3–5] PSP is defined neuropathologically by straight filaments of aggregated hyperphosphorylated tau that form morphologically distinct lesions (eg, globose neurofibrillary tangles, tufted astrocytes, oligodendroglial coiled bodies, neuropil threads) in neurons and glia.[1,2] These filaments consist of tau isoforms with 4 microtubule binding repeats. PSP overlaps clinically and neuropathologically with corticobasal degeneration (CBD), a 4-repeat tauopathy that has pathomorphological lesions that distinguish it from PSP (ballooned neurons, astrocytic plaques, and teeming subcortical WM tauopathy) and a more cortical distribution of pathology than PSP.[6]

An in vivo biomarker for tau pathology in PSP could have a transformative impact on diagnosis and drug development for this disorder.[7] Several candidate positron emission tomography (PET) radiotracers have recently been developed by screening for binding to Alzheimer disease (AD)-type tau pathology, which features a mix of 3- and 4-repeat tau that aggregates into paired helical filaments (PHFs).[8] One tracer, the pyrido-indole derivative ^{18}F-flortaucipir (formerly ^{18}F-AV1451 or ^{18}F-T807), has shown early promise as a marker of tau pathology in AD,[9,10] and several in vivo studies of ^{18}F-flortaucipir in smaller samples of PSP patients studied at individual centers reported increased uptake in regions expected to harbor tau pathology.[11–15] However, discrepancies have been noted between these positive in vivo results and in vitro autoradiography studies that showed high-affinity binding of ^{18}F-flortaucipir to PHF tau but low-affinity binding or no targeted binding to straight filamentous tau in PSP and CBD.[16–20]

In this study, we investigated ^{18}F-flortaucipir localization in a multicenter sample of 33 patients with PSP compared to 46 age-matched controls and 26 patients with Parkinson disease (PD). We hypothesized that: (1) compared to controls and PD patients, PSP patients would have increased ^{18}F-flortaucipir uptake in brain regions known to develop PSP tau pathology; (2) more advanced PSP patients would be associated with greater ^{18}F-flortaucipir retention; and (3) distinct ^{18}F-flortaucipir binding patterns would be observed in PSP clinical variants, consistent with clinicopathological descriptions. One patient with clinically diagnosed PSP died 9 months after PET, allowing for comparison between in vivo ^{18}F-flortaucipir retention and postmortem tau pathology. Prior studies assessed PET-to-autopsy relations for 2 additional clinical PSP patients in our cohort.[20,21]

Subjects and Methods

Study Participants

Thirty-three PSP patients, 26 PD patients, and 46 age-matched controls were recruited from multiple sites (Table 1). This included 10 PSP patients from the University of California, San Francisco (UCSF) who underwent magnetic resonance imaging (MRI) at UCSF and PET imaging at Lawrence Berkeley National Laboratory (LBNL); 26 PD patients and 20 controls who underwent MRI imaging at the University of California, Berkeley or LBNL and PET imaging at LBNL; 19 PSP patients and 17 controls who received MRI and PET imaging as part of 2 multicenter imaging trials sponsored by Avid Radiopharmaceuticals (NCT02167594/18F-AV-1451-A09: 19 PSP and 2 controls; NCT02016560/AV-1451-A05: 15 controls); and 4 PSP patients and 9 controls who underwent MRI and PET imaging at Massachusetts General Hospital (MGH). Control subjects were physically healthy, cognitively normal on neuropsychological testing, and had no history of parkinsonian disorder. Patients underwent a medical history, physical examination, structured caregiver interview, and neuropsychological testing. Clinical diagnosis of PSP patients was established according to the National Institute of Neurological Disorders and Stroke (NINDS)–Society for Progressive Supranuclear Palsy criteria for probable or possible PSP, as modified for the Neuroprotection and Natural History in Parkinson Plus Syndromes clinical trial.[22,23] PD patients were diagnosed according to the U.K. Parkinson's Disease Society Brain Bank clinical criteria, and were assessed for cognitive impairment as recommended by the Movement Disorder Society Task Force guidelines.[24,25] Patients were excluded if they met core clinical criteria for any other dementia, had a family history or known mutation associated with another neurodegenerative disease, or had clinically significant cerebrovascular disease or major systemic disease. Patients and controls who were enrolled in the Avid Radiopharmaceuticals imaging trials were also excluded on the basis of amyloid-β (Aβ) PET positivity, whereas Aβ PET-positive patients but not controls were included in the LBNL and MGH cohorts. The study was approved by the institutional review board of each participating site, and all subjects or their assigned surrogates gave informed consent prior to enrollment.

Clinical Evaluation

Global disease severity for 32 of 33 PSP patients was measured using the PSP Rating Scale (PSPRS), which is scored from 0 to

TABLE 1. Subject Characteristics

Characteristic	PSP	PD	Control
No.	33	26	46
Site	10 UCSF/LBNL, 19 Avid A09, 4 MGH	26 UCSF/LBNL	20 UCB/LBNL, 2 Avid A09, 15 Avid A05, 9 MGH
Age, yr	69.6 ± 5.7	67.1 ± 5.4	69.6 ± 5.4
Sex, M/F	23/10	14/12	25/21
Aβ PET, + /−	6/26 (1 NA)	5/21	0/46
MMSE	25.6 ± 3.4 (1 NA)	—	29.2 ± 0.9 (9 NA)
PSPRS	34.7 ± 11.6 (1 NA)	—	—
UPDRS	23.2 ± 10.1 (24 NA)	26.1 ± 11.4	—

Values reported are mean ± standard deviation.
Aβ = amyloid-β; F = female; LBNL = Lawrence Berkeley National Laboratory; M = male; MGH = Massachusetts General Hospital; MMSE = Mini-Mental State Examination; NA = not available; PET = positron emission tomography; PSPRS = Progressive Supranuclear Palsy Rating Scale; UCSF = University of California, San Francisco; UPDRS = Unified Parkinson's Disease Rating Scale.

100 in order of increasing severity.[26] PSP patients (32 of 33) were also tested for cognitive performance on the Mini-Mental State Examination (MMSE), and a subset of 9 PSP patients from UCSF were tested on the motor components of the Unified Parkinson's Disease Rating Scale (UPDRS). PD patients were tested on the motor components of the UPDRS. Controls were tested on the MMSE (37 of 46) or Montreal Cognitive Assessment (9 of 46). All clinical scales were assessed within 1 year of PET imaging.

The 10 PSP patients who were recruited at UCSF were assessed for variant clinical presentations based on a blinded, retrospective chart review by an expert clinician (G.D.R.), following new clinical diagnostic criteria from the Movement Disorder Society.[27] Six patients were classified with PSP-RS, 3 with PSP-PAGF, and 1 with PSP-CBS. Medical charts for the remaining PSP patients were not available for this study.

Image Data Acquisition and Processing

MRI scans were acquired for all subjects using a T1-weighted magnetization prepared rapid gradient echo sequence on a 3T (24 PSP, 29 controls) or 1.5T (9 PSP, 26 PD, 17 controls) scanner. Subjects underwent Aβ PET imaging with ^{11}C-Pittsburgh compound B (^{11}C-PiB PET; 13 PSP, 26 PD, 29 controls) or ^{18}F-florbetapir (19 PSP, 17 controls) and tau PET imaging with ^{18}F-flortaucipir, using 11 PET scanners across sites. All scans for a given subject were collected within a 1-year timeframe. Aβ PET scans were assessed for Aβ plaque positivity by applying a quantitative threshold or by visual assessment by a trained clinician, using methods that have been previously described and validated against postmortem neuropathology.[28,29] One PSP patient did not undergo Aβ PET imaging.

For tau PET imaging, approximately 10mCi of ^{18}F-flortaucipir was intravenously injected, and 4 × 5-minute frames of data were collected 80 to 100 minutes postinjection, a time window where standardized uptake value ratio (SUVR) measurement correlates well with quantification from dynamic acquisition and full compartmental modeling approaches.[30,31] ^{18}F-flortaucipir data were reconstructed and corrected for motion using site-specific protocols, and subsequent processing was done using Statistical Parametric Mapping 12 (SPM12) software except where otherwise noted. Briefly, ^{18}F-flortaucipir frames were realigned, averaged across the 80- to 100-minute time window, and coregistered to each subject's T1-weighted MRI. Voxelwise SUVR images were created by normalizing ^{18}F-flortaucipir values by the mean ^{18}F-flortaucipir uptake in a cerebellar gray matter reference region that excluded dentate nucleus, defined in native MRI space using FreeSurfer 5.1 software. Next, MRIs were skull-stripped and warped to the Montreal Neurological Institute (MNI) 152 T1-weighted template at 2mm isotropic resolution, and the resulting nonlinear transformations were used to warp ^{18}F-flortaucipir SUVR images into MNI space. Finally, ^{18}F-flortaucipir scans were smoothed prior to analysis using an 8mm isotropic full-width at half-maximum Gaussian kernel.

^{18}F-Flortaucipir Voxelwise and Region of Interest Analyses

Voxelwise 2-sample *t* tests were performed in SPM12 to assess differences in ^{18}F-flortaucipir uptake between PSP patients and controls and between PSP patients and PD patients. We used a whole brain explicit mask and added age as a nuisance regressor, as several studies have reported age-related off-target binding of ^{18}F-flortaucipir in subcortical regions relevant to PSP and PD pathology.[9,19,32] Although the number of study sites precluded adding covariates for PET scanner models, voxelwise models between PSP patients and controls were tested separately in each cohort to assess the robustness of our results irrespective of site. Also, because some PSP and PD patients were

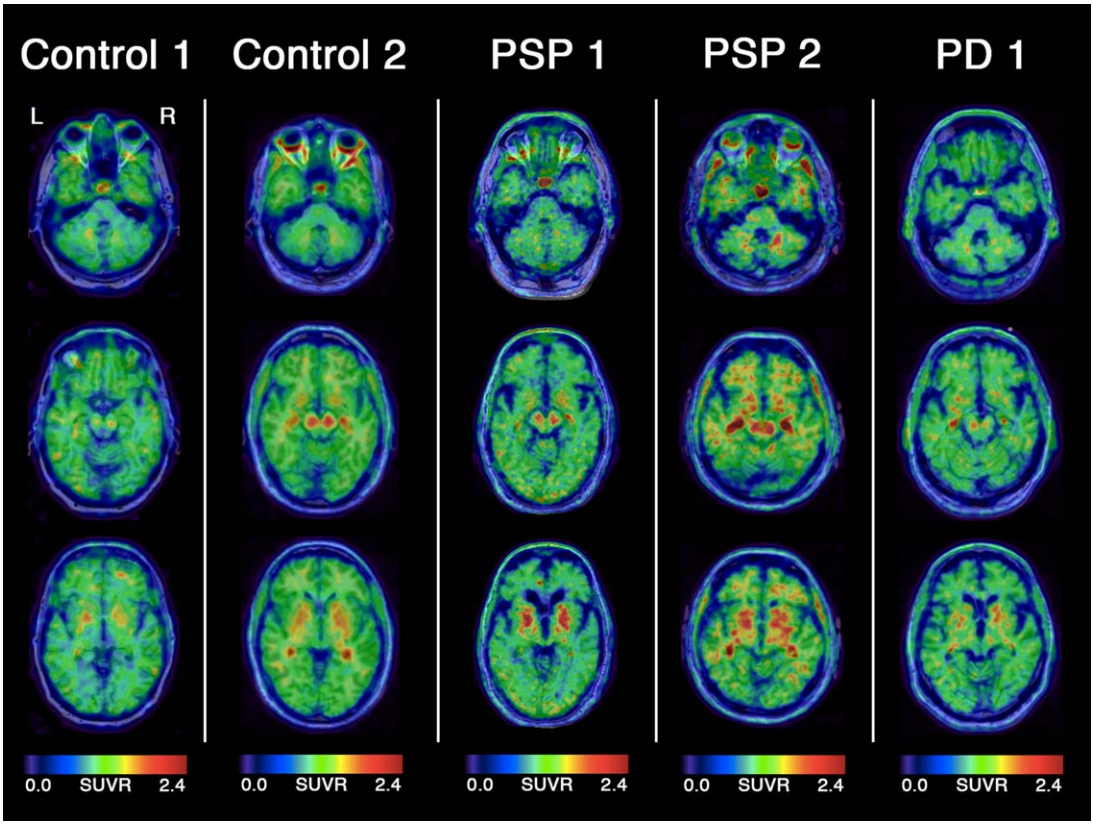

FIGURE 1: Example ^{18}F-flortaucipir scans. ^{18}F-flortaucipir standardized uptake value ratio (SUVR) images are overlaid on native-space MRIs for 5 example subjects. Far left: A 74-year-old, female healthy control with relatively low subcortical off-target positron emission tomography (PET) uptake for the control population. Second from left: A 68-year-old, male control subject with high off-target PET uptake. Middle: A 65-year-old, male progressive supranuclear palsy (PSP) patient (PSP Rating Scale [PSPRS] = 41, Mini-Mental State Examination [MMSE] = 23) with low PET uptake among the PSP patients. Second from right: A 78-year-old, male PSP patient (PSPRS = 20, MMSE = 24) with high PET uptake. Far right: A 71-year-old, male Parkinson disease (PD) patient (Unified Parkinson's Disease Rating Scale = 27) with average PET uptake among the PD patients. L = left; R = right.

Aβ PET-positive and all controls were Aβ PET negative, secondary analyses were performed with Aβ PET-positive patients removed.

Additionally, we assessed the mean ^{18}F-flortaucipir SUVR within 8 regions of interest (ROIs) that are identified in the NINDS neuropathological criteria for PSP as having moderate to high tau burden (caudate nucleus, dentate nucleus of the cerebellum, globus pallidus, pons, putamen, red nucleus, substantia nigra, and subthalamic nucleus).[2] An MNI-space version of the Talairach atlas was used to define all ROIs except for dentate nucleus, which was defined using an established cerebellar atlas (also in MNI space) that better captured this region.[33,34] Differences in ROI uptake between groups were assessed using Kruskal–Wallis tests with post hoc Mann–Whitney *U* tests. To further quantify differences in globus pallidus PET uptake for PSP patients relative to controls and PD patients, we used the R package pROC to perform receiver operating characteristic (ROC) curve analysis, utilizing the Youden index (which maximizes sensitivity + specificity) to select optimal thresholds. Primary group comparisons and ROC analyses were repeated using data corrected for partial volume effects using the geometric transfer matrix approach, as previously described.[10,35]

Neuropathology

We compared the distribution of in vivo ^{18}F-flortaucipir binding to the postmortem distribution of tau pathology as assessed by immunohistochemistry in a 64-year-old, right-handed woman with PSP-RS who died during the course of the study, 2 years after symptom onset. The patient was last seen at the UCSF memory clinic 6 months prior to death and had undergone ^{18}F-flortaucipir imaging 9 months prior to death. Brain autopsy was performed at the UCSF Neurodegenerative Disease Brain Bank, and a neuropathological evaluation was performed as previously described.[36–38] Tissue sections from the left cerebral hemisphere, right cerebellar hemisphere, and brainstem were stained with hematoxylin–eosin to assess microvacuolation, gliosis, and neuronal loss. Immunohistochemistry for phosphorylated tau (CP13, 1:1,000, mouse monoclonal, gift from Dr Peter Davies), 3-repeat tau (3R, antimouse, 1:500, Millipore, Billerica, MA), Aβ (anti–amyloid β, antimouse, 1:250, Millipore), TDP-43 (antirabbit, 1:4,000, Proteintech Group, Chicago, IL), and α-synuclein (antimouse, 1:1,000, Millipore) was carried out. Sections stained for phosphorylated tau were scored on a 3-point scale for absent (0), mild (1), moderate (2), or severe (3) levels of neurofibrillary tangles, other neuronal cytoplasmic inclusions, astrocytic plaques,

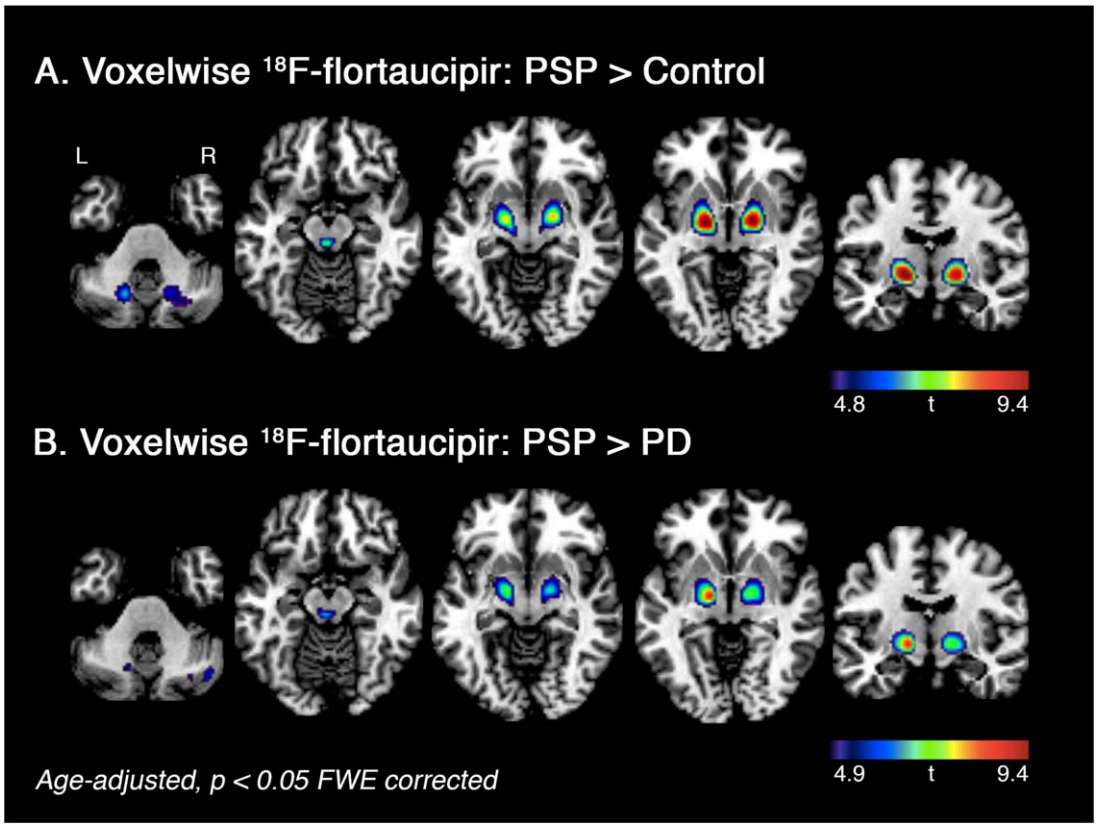

FIGURE 2: Voxelwise contrasts of ^{18}F-flortaucipir uptake. Voxelwise contrasts show regions where ^{18}F-flortaucipir uptake was greater in progressive supranuclear palsy (PSP) patients relative to controls (A) and Parkinson disease (PD) patients (B). Models were adjusted for age as a nuisance covariate, and the resulting *t* score maps are shown at familywise error (FWE)-corrected $p < 0.05$ with no cluster size correction.

other glial cytoplasmic inclusions, and gray and white matter neuropil thread or grain pathology. Pathological assessment was performed blinded to ^{18}F-flortaucipir results.

Results

Subject Characteristics and Cognitive Test Performance

Patient groups and controls did not differ on the basis of age or sex. Most PSP patients were in a mild-to-moderate clinical disease stage as indicated by performance on the PSPRS (34.7 ± 11.6, min = 15, max = 63), MMSE (25.6 ± 3.4, min = 16, max = 30), and UPDRS (n = 9, 23.2 ± 10.1, min = 13, max = 40). PD patients were also in a mild-to-moderate disease stage (UPDRS: 26.1 ± 11.4, min = 8, max = 45), and 11 of 26 were classified as having mild cognitive impairment. Six PSP-RS patients and 5 PD patients were Aβ PET-positive, whereas all controls were Aβ negative. Although Aβ PET-positive patients were included in the main analyses, we performed secondary analyses with Aβ PET-positive patients removed to ensure that findings were not driven by AD pathology.

Example ^{18}F-Flortaucipir Uptake in Individual Subjects

Figure 1 shows a selection of ^{18}F-flortaucipir SUVR images overlaid on native-space MRIs. We sought to show a representative sample by selecting controls and PSP patients who fell within the bottom and top quartiles of PET uptake, whereas the scan for 1 PD patient is representative of the average uptake seen in this group. ^{18}F-flortaucipir scans for controls showed relatively low cortical and WM retention along with consistent, but variable, degrees of tracer uptake in the choroid plexus, basal ganglia, substantia nigra, and to a lesser degree dentate nucleus of the cerebellum. This pattern, often referred to as "off-target" binding, partially overlapped with the distribution and degree of binding seen in patients with PSP, as reported previously.[11,17,19] ^{18}F-flortaucipir scans of PD patients resembled control scans.

Voxelwise Comparisons of ^{18}F-Flortaucipir Uptake

Voxelwise contrasts showed PSP patients had bilaterally elevated ^{18}F-flortaucipir uptake compared to controls in regions that are commonly associated with high PSP tau pathology (Fig 2A). At a strict multiple comparison

TABLE 2. ^{18}F-Flortaucipir SUVRs in ROIs

ROI	PSP	PD	Control
Non–partial volume-corrected SUVRs			
Caudate nucleus	0.84 ± 0.17	0.95 ± 0.14	0.96 ± 0.14
Dentate nucleus	1.29 ± 0.09[a,b]	1.19 ± 0.09	1.18 ± 0.09
Globus pallidus	1.67 ± 0.18[a,c]	1.40 ± 0.14	1.43 ± 0.12
Pons	0.91 ± 0.08	0.94 ± 0.06	0.94 ± 0.06
Putamen	1.51 ± 0.14[b,d]	1.38 ± 0.12	1.39 ± 0.13
Red nucleus	1.37 ± 0.13[d,e]	1.28 ± 0.11	1.27 ± 0.13
Substantia nigra	1.40 ± 0.13[b,f]	1.29 ± 0.10[g]	1.35 ± 0.10
Subthalamic nucleus	1.46 ± 0.12[a,c]	1.29 ± 0.10	1.31 ± 0.11
Partial volume-corrected SUVRs			
Caudate nucleus	0.39 ± 0.42	0.67 ± 0.31	0.74 ± 0.35
Dentate nucleus	2.04 ± 0.42[a,c]	1.51 ± 0.32	1.53 ± 0.32
Globus pallidus	2.33 ± 0.37[a,c]	1.63 ± 0.27[g]	1.71 ± 0.18
Pons	0.90 ± 0.14	0.89 ± 0.11[g]	0.95 ± 0.11
Putamen	1.88 ± 0.25[b,d]	1.66 ± 0.23	1.69 ± 0.23
Red nucleus	2.28 ± 0.83[e,f]	1.84 ± 0.71	1.72 ± 0.76
Substantia nigra	3.80 ± 1.28[e]	2.95 ± 0.95[h]	4.05 ± 0.92
Subthalamic nucleus	2.94 ± 0.93[a,c]	1.60 ± 0.57	1.31 ± 0.65

SUVRs are shown prior to (top) and after (bottom) correction for partial volume effects. Values reported are mean ± standard deviation. Pairwise differences were assessed with Mann–Whitney *U* tests.

[a] $p < 0.0001$, PSP > control.
[b] $p < 0.001$, PSP > PD.
[c] $p < 0.0001$, PSP > PD.
[d] $p < 0.001$, PSP > control.
[e] $p < 0.05$, PSP > PD.
[f] $p < 0.05$, PSP > control.
[g] $p < 0.05$, PD < control.
[h] $p < 0.0001$, PD < control.

PD = Parkinson disease; PSP = progressive supranuclear palsy; ROI = region of interest; SUVR = standardized uptake value ratio.

threshold ($p < 0.05$ familywise error [FWE] corrected), this included the dentate nucleus, dorsal midbrain, subthalamic nucleus, and a hotspot encompassing globus pallidus that extended into portions of the putamen and thalamus. At a more liberal statistical threshold ($p < 0.001$ uncorrected), voxelwise differences were also observed in subcortical WM near the precentral gyrus and in cerebellar WM, consistent with reports of mild tau pathology in these regions, especially with advancing PSP severity.[3] Similar results were obtained with and without age correction, when excluding Aβ PET-positive PSP patients from the analysis, and when running separate models within the LBNL, Avid Radiopharmaceuticals, and MGH cohorts (data not shown).

We observed a similar pattern of results in voxelwise comparisons of ^{18}F-flortaucipir uptake in PSP relative to PD patients (Fig 2B). Specifically, PSP patients had bilaterally increased uptake in dorsal midbrain, subthalamic nucleus, and globus pallidus at $p < 0.05$ FWE correction, along with increases in dentate nucleus, cerebellar WM, and putamen at $p < 0.001$ uncorrected.

^{18}F-Flortaucipir in ROIs

Next, we assessed the degree of ^{18}F-flortaucipir uptake in 8 subcortical regions for PSP patients, PD patients, and control subjects (Table 2, Fig 3). These data were in

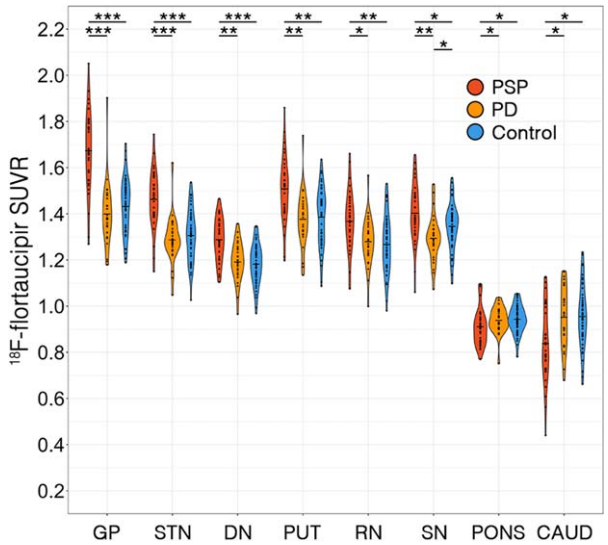

FIGURE 3: ^{18}F-flortaucipir standardized uptake value ratios (SUVRs) in regions of interest (ROIs). Violin plots show the distribution of ^{18}F-flortaucipir SUVRs in 8 ROIs for progressive supranuclear palsy (PSP) patients (red), Parkinson disease (PD) patients (orange), and control subjects (blue). Dots are used to depict individual subject SUVRs, and horizontal bars show the group means for each ROI. SUVRs in the figure are not corrected for partial volume effects. Significant Mann–Whitney *U* tests between diagnostic groups are indicated at the top: *$p<0.05$, **$p<0.001$, ***$p<0.0001$. ROIs are listed left to right in ascending order of probability values for the PSP > control contrast. SUVR means and standard deviations for each ROI are listed in Table 2. CAUD = caudate nucleus; DN = dentate nucleus; GP = globus pallidus; PUT = putamen; RN = red nucleus; SN = substantia nigra; STN = subthalamic nucleus.

agreement with the voxelwise results, and showed that PSP patients had strongly significant increases in ^{18}F-flortaucipir uptake in the globus pallidus, subthalamic nucleus, and dentate nucleus relative to controls and PD patients ($p < 0.0001$), along with moderately significant increases in the putamen ($p < 0.001$), red nucleus ($p < 0.001$ vs controls, $p < 0.05$ vs PD patients), and substantia nigra ($p < 0.05$ vs controls, $p < 0.001$ vs PD patients). PSP patients did not have greater ^{18}F-flortaucipir uptake in pons or caudate nucleus, in contrast with the expected neuropathology. Consistent with an earlier report, substantia nigra was the only region where ^{18}F-flortaucipir uptake differed between PD patients and controls (lower uptake in PD), possibly due to the loss of neuromelanin-containing neurons, which may be an off-target binding site of ^{18}F-flortaucipir.[39] Group SUVR comparisons with partial volume-corrected data yielded equivalent results (see Table 2).

As globus pallidus stood out as the region with the highest mean ^{18}F-flortaucipir retention in PSP (SUVR = 1.67 ± 0.18) and showed the greatest separation from controls, we sought to quantify the degree to which PET uptake in this region distinguished PSP from controls and PD at the single-subject level using ROC curve analysis. At an optimal SUVR threshold of 1.58, PSP patients were separated from controls with 72.7% sensitivity and 93.5% specificity on the basis of globus pallidus uptake (area under the curve [AUC] = 0.872, 95% confidence interval [CI] = 0.783–0.960), and at a slightly lower threshold of 1.52, PSP patients were separated from PD patients with 84.8% sensitivity and 92.3% specificity (AUC = 0.893, 95% CI = 0.796–0.990). ROC analyses with partial volume-corrected data gave similar results (PSP vs controls, AUC = 0.930; PSP vs PD, AUC = 0.936).

^{18}F-Flortaucipir Relations with PSP Disease Severity and Clinical Variant

Contrary to our hypothesis, voxelwise regression models ($p < 0.001$ uncorrected) in PSP patients revealed that there were no brain regions where greater ^{18}F-flortaucipir retention was correlated with increasing disease severity, as measured by higher PSPRS or lower MMSE score.

Neuropathological studies have found that clinical variants of PSP are associated with distinct distributions of tau pathology.[4,5] To consider this possibility, we visually assessed ^{18}F-flortaucipir binding patterns in 10 PSP patients who were clinically classified as PSP-RS (n = 6), PSP-PAGF (n = 3), or PSP-CBS (n = 1). Although the spatial extent and degree of ^{18}F-flortaucipir uptake varied from subject to subject, in general PSP-RS patients had bilaterally elevated uptake throughout the basal ganglia, midbrain, and dentate nucleus (Fig 4A). In contrast, all 3 PSP-PAGF patients had high basal ganglia ^{18}F-flortaucipir retention with no observable uptake in dentate nucleus (Fig 4B), consistent with the reported neuropathology of this syndrome.[3] Finally, the PSP-CBS patient showed an atypically asymmetric pattern of ^{18}F-flortaucipir uptake with greatest retention in the right dentate nucleus and left midbrain, subthalamic nucleus, globus pallidus, and putamen (Fig 4C). Lower levels of ^{18}F-flortaucipir binding were also observed in left > right frontoparietal subcortical WM. This pattern of asymmetry matched the clinical presentation, which began with a right-handed apraxia that progressed to apraxia and dystonia of the right upper limb, along with features of more classic Richardson syndrome.

Neuropathology

Figure 5 shows a comparison of in vivo ^{18}F-flortaucipir uptake versus postmortem tau immunohistochemistry in a 64-year-old woman whose primary symptoms were blurred vision with supranuclear gaze palsy (worst downward), increased axial tone, and later evolution of

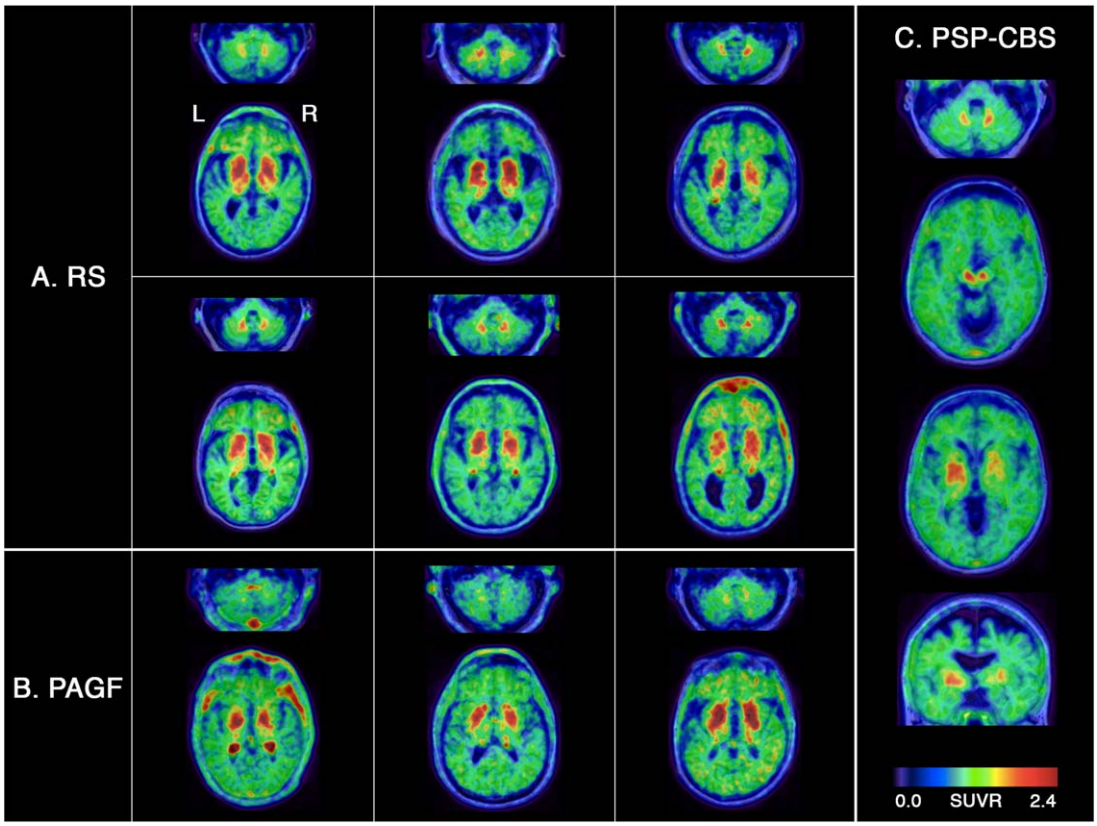

FIGURE 4: **^{18}F-flortaucipir patterns in typical and variant progressive supranuclear palsy (PSP).** ^{18}F-flortaucipir standardized uptake value ratio (SUVR) images are overlaid on native-space magnetic resonance imagines for 6 PSP–Richardson syndrome (RS) patients (A), 3 PSP–pure akinesia with gait freezing (PAGF) patients (B), and 1 PSP–corticobasal syndrome (CBS) patient (C). L = left; R = right.

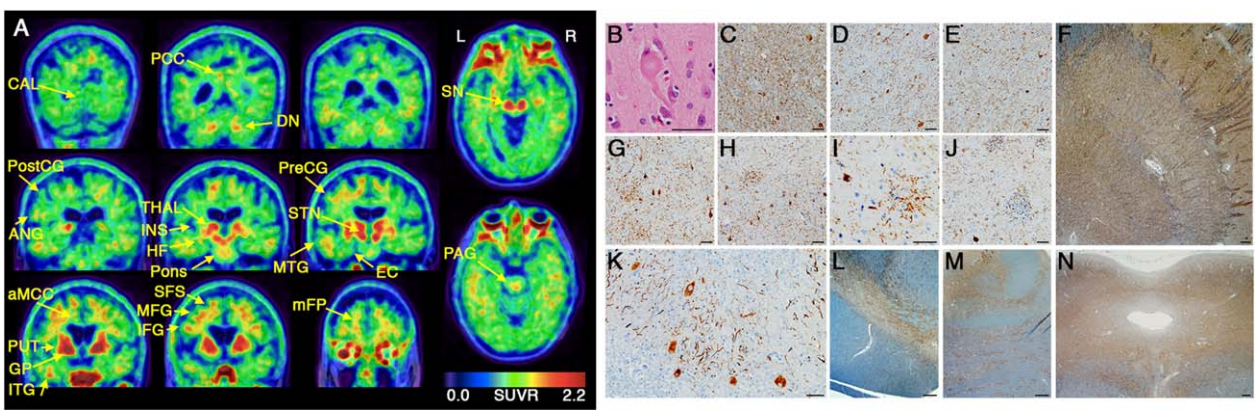

FIGURE 5: **Positron emission tomography (PET) to autopsy comparisons.** ^{18}F-flortaucipir standardized uptake value ratio (SUVR) images are shown alongside microscopic findings for a 64-year-old woman with progressive supranuclear palsy–Richardson syndrome due to corticobasal degeneration (CBD). (A) Coronal PET slices are shown from most posterior (top left) to most anterior (bottom right). (B) A ballooned neuron typical of CBD is shown on hematoxylin–eosin stain. Hyperphosphorylated tau immunohistochemistry (CP13) shows neuronal cytoplasmic inclusions and white matter thread pathology in the subthalamic nucleus (C), thalamus (D), globus pallidus interna (E), lentiform nucleus (F), superior frontal sulcus (G), precentral gyrus (H), angular gyrus (I), caudate nucleus (J), dentate nucleus (K), substantia nigra (L), pons (M), and midbrain tectum (N). Astrocytic plaques are visible in G–I. Scale bars: 50 μm (B–E, G–K) and 500 μm (F, L–N). aMCC = anterior midcingulate cortex; ANG = angular gyrus; CAL = calcarine cortex; DN = dentate nucleus; EC = entorhinal cortex; GP = globus pallidus; HF = hippocampal formation; IFG = inferior frontal gyrus; INS = insula; ITG = inferior temporal gyrus; L = left; MFG = middle frontal gyrus; mFP = medial frontal pole; MTG = middle temporal gyrus; PAG = periaqueductal gray; PCC = posterior cingulate cortex; PostCG = postcentral gyrus; PreCG = precentral gyrus; PUT = putamen; R = right; SFS = superior frontal sulcus; SN = substantia nigra; STN = subthalamic nucleus; THAL = thalamus.

cognitive slowing and backward falls consistent with PSP-RS (PSPRS = 47, MMSE = 16 at clinical evaluation proximate to PET). MRI revealed lateral ventricular enlargement and pronounced, bilateral atrophy of the midbrain, frontoparietal and cingulate cortices, with scattered WM hyperintensities. ^{11}C-PiB PET did not show evidence of elevated cortical amyloid. The ^{18}F-flortaucipir scan showed a bilateral pattern of uptake that was consistent with but more spatially extensive than the ^{18}F-flortaucipir scans for most PSP patients in our cohort. This included highest tracer binding in the globus pallidus and additionally high uptake in the putamen, subthalamic nucleus, midbrain, and dentate nucleus (see Fig 5A). In contrast to most PSP patients, we also observed elevated ^{18}F-flortaucipir uptake in the thalamus, caudate nucleus, and frontal lobe (WM more than cortex), with slight elevation in the pons.

Brain autopsy revealed characteristic findings of CBD (see Fig 5B).[40] The pattern of neuronal loss and gliosis matched the clinical presentation of PSP-RS with greatest involvement of midbrain nuclei, along with basal ganglia, superior frontal sulcus, and precentral gyrus. Tau immunohistochemistry revealed mostly severe levels of glial and neuronal cytoplasmic inclusions and neuropil thread pathology throughout subcortical regions with high ^{18}F-flortaucipir binding, including globus pallidus, striatum, thalamus, subthalamic nucleus, midbrain, pons, and dentate nucleus (Table 3, see Fig 5C–N). Most cortical regions also had severe cytoplasmic and neuropil tau pathology and were distinguished from subcortical regions by the presence of astrocytic plaques. The density of tau immunostaining appeared greatest in frontal, perirolandic, and posterior cingulate regions that corresponded with elevated ^{18}F-flortaucipir. However, moderate-to-severe tau pathology was also observed in the insula and postcentral gyrus despite unremarkable ^{18}F-flortaucipir binding. Calcarine cortex was the only region examined with no detectable tau pathology, and showed no ^{18}F-flortaucipir elevation. Three-repeat tau immunohistochemistry revealed age-related neurofibrillary tangles and threads confined to entorhinal cortex (Braak stage 1). Immunostaining for Aβ, TDP-43, and α-synuclein was negative.

Discussion

In this study, we assessed the novel tau PET radiotracer ^{18}F-flortaucipir in 33 patients with clinically diagnosed PSP who were recruited at multiple sites. Voxelwise ($p < 0.05$ FWE corrected) and ROI analyses revealed that relative to age-matched controls and PD patients, PSP patients had bilaterally elevated ^{18}F-flortaucipir uptake in globus pallidus, subthalamic nucleus, midbrain, and dentate nucleus of the cerebellum, with globus pallidus having the highest overall uptake and best group separation. These results were consistent when performing analyses with and without correction of PET data for partial volume effects. No group differences in ^{18}F-flortaucipir uptake were observed in pons or caudate nucleus, and although some PSP patients appeared to show tracer elevation in subcortical WM and parts of the neocortex, we did not observe strong group-level differences in these regions. Although a wide dynamic range was found in both the degree and spatial extent of ^{18}F-flortaucipir binding in PSP, clinical severity did not correlate with tracer uptake in any brain region. Encouragingly, we did find differences in the pattern of ^{18}F-flortaucipir binding within typical and variant PSP presentations, including sparing of dentate nucleus in PSP-PAGF and asymmetric binding in PSP-CBS. Together, these results indicate a close correspondence between the expected neuropathology of PSP and the pattern of elevated ^{18}F-flortaucipir uptake that we observed in vivo. Finally, there was colocalization between ^{18}F-flortaucipir uptake and postmortem tau pathology in a patient with clinical PSP due to underlying CBD.

An imaging biomarker of tau pathology in PSP could contribute to earlier and more accurate diagnosis, hasten drug development through improved screening and assessment of drug target engagement, and aid basic research efforts, analogous to the multifaceted impact of Aβ PET on AD research over the past decade.[41] PSP is also considered a primary target for proof-of-concept testing of tau therapeutics, which may have broader applications in AD and other tauopathies.[7] Whereas previous studies have reported preliminary ^{18}F-flortaucipir findings in relatively small numbers of PSP patients studied at single sites, our study found that ^{18}F-flortaucipir PET provided robust group-level differences and strong single-subject discrimination between PSP and both normal and disease (PD) controls when combining data across multiple sites and PET scanner models.[11–15] The most consistent finding when comparing PSP patients to controls across studies has been bilaterally elevated ^{18}F-flortaucipir uptake in the globus pallidus. Elevated uptake in subthalamic nucleus and dorsal midbrain is also a consistent feature, along with the relative absence of tracer retention in pons, cortex, and subcortical WM, whereas uptake in dentate nucleus has been variable. Associations of ^{18}F-flortaucipir signal with composite measures of disease severity have been inconsistent,[11–13,15] which may be explained by disease heterogeneity in both topographic patterns of binding and clinical progression. We identified potential differences in binding patterns between distinct clinical variants of PSP (PSP-PAGF and PSP-CBS compared to PSP-RS) corresponding to reported differences in the distribution of tau pathology across these variants at autopsy,[3] although these findings need to be replicated in larger samples. Further work is

TABLE 3. Semiquantitative Scoring of Tau Immunohistochemistry in Progressive Supranuclear Palsy–Richardson Syndrome/Corticobasal Degeneration Autopsy Case

Region	NFTs	NCIs	APs	GCIs	GM Thread	WM Thread
Angular gyrus	0	3	3	3	3	3
Ant. midcingulate	0	2	1	3	2	3
Calcarine cortex	0	0	0	0	0	0
Dentate nucleus	0	3	0	3	3	1
Entorhinal cortex	2	3	2	2	3	3
Globus pallidus	0	2	0	3	3	NA
Hippocampus						
CA1/subiculum	0	3	0	0	3	NA
CA2	0	2	0	0	1	NA
CA3–4	0	2	0	0	1	NA
Dentate gyrus	0	3	0	0	0	1
Inf. frontal gyrus	0	3	3	3	3	3
Inf. temporal gyrus	0	3	3	3	3	2
Med. frontal pole	0	3	3	3	3	3
Mid. frontal gyrus	0	3	3	3	3	3
Mid. insula	0	3	3	3	3	3
Mid./Sup. temporal	0	3	3	2	3	2
Periaqueductal GM	0	3	0	2	3	NA
Pontine nuclei	0	2	0	0	3	1
Post. cingulate	0	3	3	3	3	3
Postcentral gyrus	0	2	2	2	2	2
Precentral gyrus	0	3	3	3	3	3
Putamen	0	3	0	1	3	3
Sub. nigra	0	3	0	3	3	NA
Subthalamic nucleus	0	3	0	2	3	NA
Sup. frontal sulcus	0	3	3	3	3	3
Thalamus	0	2	2	2	3	2

The degree of regional phosphorylated tau pathology was scored on a 3-point scale as absent (0), mild (1), moderate (2), or severe (3).
Ant. = anterior; AP = astrocytic plaque; GCI = other glial cytoplasmic inclusion; GM = gray matter; Inf. = inferior; Med. = medial; Mid. = middle; NA = not applicable; NCI = other neuronal cytoplasmic inclusion; NFT = neurofibrillary tangle; Post. = posterior; Sub. = substantia; Sup. = superior; WM = white matter.

also needed to assess the utility of ^{18}F-flortaucipir in aiding with difficult differential diagnoses within the PSP spectrum, such as the discrimination of PSP-P from PD.

Unfortunately, off-target tracer binding in normal and disease controls (eg, PD, AD) overlaps with and complicates the interpretation of tracer binding in several subcortical ROIs. Midbrain binding in healthy older controls may reflect binding to neuromelanin-containing cells in the substantia nigra,[17,19] a finding supported by lower levels of nigral binding in PD in our study and others.[13,39] The cause of off-target binding in other subcortical structures (putamen, pallidum, and to a lesser degree thalamus and cerebellum), which correlates with age and is independent of Aβ, is not known.[9,19,32] From

a practical point of view, off-target binding may limit the utility of ^{18}F-flortaucipir in detecting early stage PSP, in which the distribution and degree of tracer binding will overlap to the greatest degree with binding in controls. The lack of specificity of ligand binding means that quantification of ^{18}F-flortaucipir in subcortical structures will always be contaminated to some degree by non–tau-related signal, which is suboptimal when considering application of ^{18}F-flortaucipir as a marker of 4-repeat tau pathological burden in observational studies and therapeutic trials. Larger samples of autopsy-confirmed subjects are needed to more precisely determine the diagnostic accuracy of ^{18}F-flortaucipir in PSP and the neuropathological stage at which ^{18}F-flortaucipir can reliably distinguish PSP patients from PD patients and controls.

Several autoradiography studies have assessed in vitro binding properties of ^{18}F-flortaucipir in PSP and other neurodegenerative pathologies.[16–20] Across postmortem binding studies, ^{18}F-flortaucipir has been found to have high affinity for AD-type PHF tau. Results in PSP and CBD have differed in subtle but important ways; some studies reported no binding on autoradiography to 4-repeat, straight filamentous tau in PSP and CBD,[17,18] whereas others found low level binding in both conditions.[19] When interpreting these in vitro results, it is important to recognize that autoradiography assays are highly sensitive to tissue preparation and experimental conditions. Our in vivo results are consistent with studies that showed low-level binding to postmortem PSP tissue,[19] perhaps reflecting low tracer affinity compared to AD that does not survive more harsh tissue preparations.[17] Importantly, off-target binding is detected by autoradiography under some but not all experimental conditions, suggesting that some assays may yield false negatives in predicting in vivo tracer performance.[17,19] The regionally specific increases in ^{18}F-flortaucipir uptake that were observed in PSP in our study and others,[11–13] and the correspondence between antemortem tracer retention and postmortem tau pathology in the patient in our study with autopsy-confirmed CBD, are difficult to reconcile with a conclusion that ^{18}F-flortaucipir has no specific binding to 4-repeat tauopathies. Although we cannot rule out the possibility of tracer binding to a process that strongly colocalizes with 4-repeat tau pathology, the absence of elevated uptake in PD patients argues against a more nonspecific binding to other misfolded protein aggregates or neurodegenerative markers.

In vivo ^{18}F-flortaucipir has been previously compared against postmortem neuropathology in a small number of PSP and CBD patients, including 2 clinical PSP patients from our cohort. A study of 2 patients with PSP pathology (including 1 patient from our cohort) found colocalization of tau aggregates with in vivo PET signal, but no correlation between regional ^{18}F-flortaucipir uptake and the degree of tau pathology as measured by immunohistochemistry.[16,20] Additionally, 2 case reports in autopsy-confirmed CBD patients (including 1 clinical PSP patient from our cohort) found significant correlations between ^{18}F-flortaucipir uptake and tau pathological burden.[21,42] The CBD case that we presented here is consistent with these earlier reports, showing colocalization between in vivo ^{18}F-flortaucipir and postmortem tau pathology. However, the PET-to-autopsy comparisons presented in this study are limited in that we did not compare PET uptake to continuous, quantitative measures of tau pathology. There is a need to perform more quantitatively rigorous assessments of tau PET relations with neuropathology in larger groups of patients with clinical PSP, CBD, and other non-AD tauopathies.[43]

Although our data support continued exploration of ^{18}F-flortaucipir in PSP, the tracer also has clear limitations, and tau radiotracers are needed that show greater sensitivity and specificity for the disease. In vitro and initial in vivo data suggest that 2 other putative tau tracers, ^{18}F-THK5351 and ^{11}C-PBB3, may bind tau aggregates in PSP and CBD.[44,45] Unfortunately, both tracers also show off-target binding in midbrain and basal ganglia to a similar if not greater extent than ^{18}F-flortaucipir.[44,45] Furthermore, brain penetrant metabolites and photosensitivity have limited the utility of ^{11}C-PBB3,[46,47] and recent reports of ^{18}F-THK5351 binding to monoamine oxidase B have raised questions about the utility of this tracer.[48] Given that all tau tracers applied in humans to date were selected for their ability to detect PHF tau in AD tissue, it is likely that a dedicated effort will be required to identify ligands that optimally capture the distinct aggregates of PSP.

In conclusion, we report that in vivo ^{18}F-flortaucipir uptake in PSP patients is increased in many but perhaps not all of the regions that harbor tau pathology at autopsy, relative to controls and PD patients. The utility of ^{18}F-flortaucipir in PSP may ultimately be limited by lower affinity binding to PSP tau and off-target binding in subcortical regions of interest, and other PET tracers that are optimized for detecting 4-repeat tau may be needed to capture PSP and CBD pathology in a more sensitive and specific manner. Nevertheless, until such tracers are available, our data support continued exploration of ^{18}F-flortaucipir as a biomarker for tau pathology in PSP and CBD in longitudinal studies with ultimate autopsy confirmation.

Acknowledgment

This study was funded in part by Avid Radiopharmaceuticals (NCT02167594, NCT02016560). Additional support came from the NIH National Institute on Aging (R01-AG038791, U54-NS092089, P01-AG019724, K08-AG052648), the Tau Consortium, and the Michael J. Fox Foundation.

We thank K. Norton, J. O'Neil, M. Janabi, and A. Joshi for their contributions in the acquisition and analysis of imaging data. We are especially thankful for the dedication and commitment of the patients and families who participated in this research.

Author Contributions

Conception and design of the study: D.R.S., C.T.M., S.S., B.C.D., A.S., M.D.D., W.J.J., A.L.B., G.D.R. Acquisition and analysis of data: all authors. Drafting of text and figures: D.R.S., S.S., G.D.R.

Potential Conflicts of Interest

A.S. and M.D.D. are full-time employees of Avid Radiopharmaceuticals, a wholly owned subsidiary of Eli Lilly and Company, which owns ^{18}F-flortaucipir, the tau PET tracer used in this study. I.L., E.D.R., L.T.G., I.N., M.G., A.L.B., and G.D.R. receive grant support from Avid Radiopharmaceuticals. E.D.R. has a patent issued on tau reduction.

References

1. Dickson DW, Rademakers R, Hutton ML. Progressive supranuclear palsy: pathology and genetics. Brain Pathol 2007;17:74–82.
2. Hauw JJ, Daniel SE, Dickson D, et al. Preliminary NINDS neuropathologic criteria for Steele-Richardson-Olszewski syndrome (progressive supranuclear palsy). Neurology 1994;44:2015–2019.
3. Williams DR, Holton JL, Strand C, et al. Pathological tau burden and distribution distinguishes progressive supranuclear palsy-parkinsonism from Richardson's syndrome. Brain 2007;130:1566–1576.
4. Williams DR, Lees AJ. Progressive supranuclear palsy: clinicopathological concepts and diagnostic challenges. Lancet Neurol 2009; 8:270–279.
5. Dickson DW, Ahmed Z, Algom AA, et al. Neuropathology of variants of progressive supranuclear palsy. Curr Opin Neurol 2010; 23:394–400.
6. Dickson DW. Neuropathologic differentiation of progressive supranuclear palsy and corticobasal degeneration. J Neurol 1999; 246(suppl 2):II6–II15.
7. Boxer AL, Gold M, Huey E, et al. Frontotemporal degeneration, the next therapeutic frontier: molecules and animal models for frontotemporal degeneration drug development. Alzheimers Dement 2013;9:176–188.
8. Okamura N, Harada R, Furukawa K, et al. Advances in the development of tau PET radiotracers and their clinical applications. Ageing Res Rev 2016;30:107–113.
9. Johnson KA, Schultz A, Betensky RA, et al. Tau positron emission tomographic imaging in aging and early Alzheimer disease. Ann Neurol 2016;79:110–119.
10. Ossenkoppele R, Schonhaut DR, Schöll M, et al. Tau PET patterns mirror clinical and neuroanatomical variability in Alzheimer's disease. Brain 2016;139:1551–1567.
11. Smith R, Schain M, Nilsson C, et al. Increased basal ganglia binding of 18 F-AV-1451 in patients with progressive supranuclear palsy. Mov Disord 2017;32:108–114.
12. Whitwell JL, Lowe VJ, Tosakulwong N, et al. [18 F]AV-1451 tau positron emission tomography in progressive supranuclear palsy. Mov Disord 2017;32:124–133.
13. Cho H, Choi JY, Hwang MS, et al. Subcortical 18 F-AV-1451 binding patterns in progressive supranuclear palsy. Mov Disord 2017; 32:134–140.
14. Coakeley S, Cho SS, Koshimori Y, et al. Positron emission tomography imaging of tau pathology in progressive supranuclear palsy. J Cereb Blood Flow Metab 2017;37:3150–3160.
15. Passamonti L, Vázquez Rodríguez PV, Hong YT, et al. 18F-AV-1451 positron emission tomography in Alzheimer's disease and progressive supranuclear palsy. Brain 2017;140:781–791.
16. Smith R, Schöll M, Honer M, et al. Tau neuropathology correlates with FDG-PET, but not AV-1451-PET, in progressive supranuclear palsy. Acta Neuropathol 2017;133:149–151.
17. Marquié M, Normandin MD, Vanderburg CR, et al. Validating novel tau positron emission tomography tracer [F-18]-AV-1451 (T807) on postmortem brain tissue. Ann Neurol 2015;78:787–800.
18. Sander K, Lashley T, Gami P, et al. Characterization of tau positron emission tomography tracer [18F]AV-1451 binding to postmortem tissue in Alzheimer's disease, primary tauopathies, and other dementias. Alzheimers Dement 2016;12:1116–1124.
19. Lowe VJ, Curran G, Fang P, et al. An autoradiographic evaluation of AV-1451 tau PET in dementia. Acta Neuropathol Commun 2016;4:58.
20. Marquié M, Normandin MD, Meltzer AC, et al. Pathological correlations of [F-18]-AV-1451 imaging in non-Alzheimer tauopathies. Ann Neurol 2017;81:117–128.
21. McMillan CT, Irwin DJ, Nasrallah I, et al. Multimodal evaluation demonstrates in vivo 18F-AV-1451 uptake in autopsy-confirmed corticobasal degeneration. Acta Neuropathol 2016;132:935–937.
22. Litvan I, Agid Y, Calne D, et al. Clinical research criteria for the diagnosis of progressive supranuclear palsy (Steele-Richardson-Olszewski syndrome): report of the NINDS-SPSP international workshop. Neurology 1996;47:1–9.
23. Bensimon G, Ludolph A, Agid Y, et al. Riluzole treatment, survival and diagnostic criteria in Parkinson plus disorders: the NNIPPS study. Brain 2009;132:156–171.
24. Gibb WR, Lees AJ. The relevance of the Lewy body to the pathogenesis of idiopathic Parkinson's disease. J Neurol Neurosurg Psychiatry 1988;51:745–752.
25. Litvan I, Goldman JG, Tröster AI, et al. Diagnostic criteria for mild cognitive impairment in Parkinson's disease: Movement Disorder Society Task Force guidelines. Mov Disord 2012;27:349–356.
26. Golbe LI, Ohman-Strickland PA. A clinical rating scale for progressive supranuclear palsy. Brain 2007;130:1552–1565.
27. Höglinger GU, Respondek G, Stamelou M, et al. Clinical diagnosis of progressive supranuclear palsy—the Movement Disorder Society criteria. Mov Disord 2017;32:853–864.
28. Clark CM, Schneider JA, Bedell BJ, et al. Use of florbetapir-PET for imaging beta-amyloid pathology. JAMA 2011;305:275–283.
29. Villeneuve S, Rabinovici GD, Cohn-Sheehy BI, et al. Existing Pittsburgh compound-B positron emission tomography thresholds are

too high: statistical and pathological evaluation. Brain 2015;138: 2020–2033.

30. Hahn A, Schain M, Erlandsson M, et al. Modeling strategies for quantification of in vivo 18F-AV-1451 binding in patients with tau pathology. J Nucl Med 2017;58:623–631.
31. Baker SL, Lockhart SN, Price JC, et al. Reference tissue-based kinetic evaluation of 18F-AV-1451 for tau imaging. J Nucl Med 2017;58:332–338.
32. Schöll M, Lockhart SN, Schonhaut DR, et al. PET imaging of tau deposition in the aging human brain. Neuron 2016;89:971–982.
33. Diedrichsen J, Balsters JH, Flavell J, et al. A probabilistic MR atlas of the human cerebellum. Neuroimage 2009;46:39–46.
34. Lancaster JL, Woldorff MG, Parsons LM, et al. Automated Talairach atlas labels for functional brain mapping. Hum Brain Mapp 2000;10:120–131.
35. Rousset OG, Ma Y, Evans AC. Correction for partial volume effects in PET: principle and validation. J Nucl Med 1998;39:904–911.
36. Mackenzie IR, Neumann M, Baborie A, et al. A harmonized classification system for FTLD-TDP pathology. Acta Neuropathol 2011; 122:111–113.
37. Hyman BT, Phelps CH, Beach TG, et al. National Institute on Aging-Alzheimer's Association guidelines for the neuropathologic assessment of Alzheimer's disease. Alzheimers Dement 2012;8:1–13.
38. Murray ME, Cannon A, Graff-Radford NR, et al. Differential clinicopathologic and genetic features of late-onset amnestic dementias. Acta Neuropathol 2014;128:411–421.
39. Hansen AK, Knudsen K, Lillethorup TP, et al. In vivo imaging of neuromelanin in Parkinson's disease using 18F-AV-1451 PET. Brain 2016;139:2039–2049.
40. Dickson DW, Bergeron C, Chin SS, et al. Office of Rare Diseases neuropathologic criteria for corticobasal degeneration. J Neuropathol Exp Neurol 2002;61:935–946.
41. Villemagne VL, Doré V, Bourgeat P, et al. Aβ-amyloid and tau imaging in dementia. Semin Nucl Med 2017;47:75–88.
42. Josephs KA, Whitwell JL, Tacik P, et al. [18F]AV-1451 tau-PET uptake does correlate with quantitatively measured 4R-tau burden in autopsy-confirmed corticobasal degeneration. Acta Neuropathol 2016;132:931–933.
43. Armstrong MJ, Litvan I, Lang AE, et al. Criteria for the diagnosis of corticobasal degeneration. Neurology 2013;80:496–503.
44. Ishiki A, Harada R, Okamura N, et al. Tau imaging with [18F]THK-5351 in progressive supranuclear palsy. Eur J Neurol 2017;24:130–136.
45. Maruyama M, Shimada H, Suhara T, et al. Imaging of tau pathology in a tauopathy mouse model and in Alzheimer patients compared to normal controls. Neuron 2013;79:1094–1108.
46. Hashimoto H, Kawamura K, Igarashi N, et al. Radiosynthesis, photoisomerization, biodistribution, and metabolite analysis of 11C-PBB3 as a clinically useful PET probe for imaging of tau pathology. J Nucl Med 2014;55:1532–1538.
47. Kimura Y, Ichise M, Ito H, et al. PET quantification of tau pathology in human brain with 11C-PBB3. J Nucl Med 2015;56:1359–1365.
48. Ng KP, Pascoal TA, Mathotaarachchi S, et al. Monoamine oxidase B inhibitor, selegiline, reduces 18F-THK5351 uptake in the human brain. Alzheimers Res Ther 2017;9:25.